

Dissipative particle dynamics simulations on inversion dynamics of spherical micelles

Bingbing Hong, Feng Qiu,^{a)} Hongdong Zhang, and Yuliang Yang

Department of Macromolecular Science, The Key Laboratory of Molecular Engineering of Polymers, Ministry of Education, Fudan University, Shanghai 200433, China

(Received 23 March 2010; accepted 2 June 2010; published online 28 June 2010)

We simulate the inversion process of a spherical micelle composed of symmetric diblock copolymers by means of dissipative particle dynamics. The evolution of micelle morphology reveals that the inversion is a two-staged process, in which a rapid agglomeration of outer lyophobic blocks occurs first, followed by a slow penetration of inner lyophilic blocks through the porous lyophobic layer. Calculation of the radius of gyration and hydrodynamic radius indicates that an intermediate with a dilute core and a dense shell emerges in the inversion. The characteristic time of inversion scales with the block copolymer chain length with the scaling exponent ranging from 1.67 to 1.89, which can be well described by a simplified chemical-potential-driven flow model. Further simulations incorporating different denaturation times for the two types of blocks indicate the inversions do not experience molecularly scattered states, but form either collapsed intermediates or loosely associated clusters of small sizes. Possible connections of the simulations to the light scattering experiments are discussed. © 2010 American Institute of Physics.
[doi:10.1063/1.3456735]

I. INTRODUCTION

Amphiphilic block copolymers can self-assemble into various aggregations, such as micelles and vesicles, with higher stability than their small-surfactant counterparts due to the macromolecular nature. In the presence of selective solvent, they form either normal or inverted micellar/vesicular structures, depending on the relative affinities between different blocks and the solvent.¹ After complete formation of the micelles/vesicles, if the solvent is switched from being selective for the shell to for the core blocks, core-shell inversion will be induced.² In 1998, a new associable class of “schizophrenic” block copolymers came into being. Unlike common polymeric amphiphiles for which the lyophilicity/lyophobicity of each type of block is controlled by the solvent selectivity, these novel copolymers can exist in both forms of normal and inversed structures in aqueous environment if the solution temperature,^{3–6} pH,^{5–13} or ionic strength^{6,8,10,12} are carefully adjusted. That is, the block lyophilic/lyophobic characters of schizophrenic copolymers can be changed reversibly while the solvent selectivity remains unaltered. Moreover, the reversible self-assembly of schizophrenic structures in response to external stimuli may find applications in drug delivering through confined body fluid with varied pH, or ion concentrations.¹⁴

Although still quite few, researches on the dynamics of inversion between the equilibrium states do begin to emerge and may receive more attention in the future. Liu *et al.*¹⁵ have employed laser light scattering to trace the pH-induced inversion process of micelles composed of zwitterionic diblock copolymer, poly(4-vinylbenzoic acid)-*b*-poly(*N*-

(morpholino)ethyl methacrylate) (VBA-*b*-MEMA). They proposed that intermicellar association accompanies the inversion from small VBA-core to large MEMA-core micelles, and that core splitting is an indispensable pathway to reduce the large cores into small ones during the reversed process. The same group has reported another schizophrenic diblock copolymer with pure salt-responsiveness,¹⁶ and proposed a fusion mechanism for the inversion from the small-core micelles to the large-core micelles at the range of high polymer concentration. Different from the micelle inversion driven by the incompatibility between one type of block and the solvent, the pH-induced inversion of vesicles formed from zwitterionic triblock copolymers in the work of Eisenberg *et al.*¹⁷ is controlled by the preferential segregation of more interrepulsive lyophilic blocks to the outer layer and less repulsive blocks to the inside.

Recently, Chen *et al.*² investigated the core-shell reversion process of the aggregates formed by polystyrene-*b*-poly(4-vinylpyridine) and gold nanoparticles. The reversion starts from the micelles, ends in the vesiclelike morphologies, and is irreversible. They concluded that there should be no molecularly dispersed intermediates in the reversion process. Therefore, the experiment presents a complementary example to the claim of completely dissociated intermediate states of unimers of Liu *et al.*^{15,16}

Although the experiments of Chen *et al.* have presented useful concepts about inversion, direct data to support their proposed mechanisms are still in lack. Besides, basic physical problems, such as what sets the inversion time scale and what principle is involved in the inversion, remain unsolved. One suggestion¹⁵ is that it is possible to consider the inversion between small cores and large cores as a generalized version of unimer-micelle transition. That is, the unimer-

^{a)}Author to whom correspondence should be addressed. Electronic mail: fengqiu@fudan.edu.cn.

micelle transition which has been perfectly described by Aniansson–Wall theory¹⁸ is a specific case of inversion between small cores and large cores with the aggregation degree of the small-core micelles equal to one. In fact, this treatment, such as the micelle inversion experiments, deals with a complex situation coupling the inversion with micelle fusion/fission and unimer entry/expulsion.

Herein, we investigate the dynamics of micelle inversion by dissipative particle dynamics (DPD) simulation.¹⁹ We choose micelles because they have simpler structures and inversion mechanisms than vesicles do. A typical simulation begins with an artificial spherical micelle. After full equilibration, the micelle is induced to undertake a core-shell inversion process as the core turns affinitive to the solvent and the shell blocks become insoluble. The isolated spherical micelles consist of symmetric diblock copolymers, so the two inversed micellar structures are of the same size and the inversion between the two equilibrium states is well separated from the micellar fusion/fission and unimer entry into or expulsion from the micelles. Therefore, we investigate the inversion itself. The DPD method is capable of illustrating how the polymer conformations and the internal structure of micelles change with time. It could also tell what the molecular mechanism governing micelle inversion is. Since all the knowledge is hard to gain in current experiments, we expect our simulation will shed light on these queries and be instructive to the future experiments.

The paper is organized as follows: the simulation details are given in Sec. II; in Sec. III, we start from the initial states, proceed with a typical inversion process and analyze the determining factor on the inversion time scale. In addition, the inversions with different denaturation times of the shell and core blocks are compared, and some comments on the relevant experiments are made based on the simulation results. Conclusions are finally drawn in Sec. IV.

II. SIMULATION DETAILS

A. DPD techniques

The DPD employed here is a coarse-grained technique firstly introduced by Hoogerbrugge and Koelman,¹⁹ and has been extensively applied to study the mesoscopic behaviors of complex fluid systems, e.g., colloids,^{19,20} biomembranes,²¹ and polymers.^{22–25} There are three types of beads in our models, solvent bead (denoted by *s*) representing lumped small solvent molecules, the bead (labeled with *A*) standing for a polymeric segment denaturing from being lyophilic to lyophobic after the inversion begins, and the bead (labeled with *B*) for an initially lyophobic segment which turned into being lyophilic in the inversion. As the previous simulations, the bead mass m_0 , energy scale $k_B T$, length scale r_0 , and time scale $\tau = r_0(m_0/k_B T)^{1/2}$ are all set to unit. Each bead evolves under exertions of three kinds of pairwise-additive forces: (1) the conservative force \mathbf{F}_{ij}^C which characterizes each type of beads by its repulsion strengths a_{ij} with itself and other types, and takes the form $\mathbf{F}_{ij}^C = a_{ij} w(r_{ij}) \mathbf{e}_{ij}$; (2) the dissipative force, $\mathbf{F}_{ij}^D = -\gamma w^2(r_{ij})(\mathbf{e}_{ij} \cdot \mathbf{v}_{ij}) \mathbf{e}_{ij}$, which acts as a drag to slow

down the particles; and (3) the random force, $\mathbf{F}_{ij}^R = \sigma w(r_{ij}) \xi_{ij} \mathbf{e}_{ij} (\Delta t)^{-1/2}$, representing a heat source. The combined effect of (2) and (3) is a thermostat.

In the formulae for the three kinds of forces above, $\mathbf{v}_{ij} = \mathbf{v}_i - \mathbf{v}_j$, $\mathbf{r}_{ij} = \mathbf{r}_i - \mathbf{r}_j$, $r_{ij} = |\mathbf{r}_{ij}|$, $\mathbf{e}_{ij} = \mathbf{r}_{ij}/r_{ij}$, and $\Delta t = 0.01 \tau$ is the time step for numerical integration over the equations of Newtonian motion for each bead. The dimensionless weight function, $w(r) = 1 - r/r_0$ for $r \leq r_0$, and $w(r) = 0$ for $r > r_0$, is soft, allowing overlaps between beads. γ and σ are the strengths of \mathbf{F}_{ij}^D and \mathbf{F}_{ij}^R , respectively. To make the system a thermostat, they should satisfy the fluctuation-dissipation theorem $\sigma^2 = 2\gamma k_B T$. In our simulations, γ is set to be $4.5[(k_B T)m_0/r_0^2]^{1/2}$, resulting in less than 1% deviation of kinetic temperature from the predefined value. $\xi_{ij}(t)$ in \mathbf{F}_{ij}^R generates random elements that are independent for each pair of beads and for each time step, and has zero mean and unit standard deviation. The repulsion strengths between the three types of beads are chosen as $a_{ss} = a_{AA} = a_{BB} = 25k_B T/r_0$, the strength between the lyophilic bead and the solvent a_{sl} is set as $25k_B T/r_0$, the lyophobic-solvent repulsion strength a_{sb} varies from $40k_B T/r_0$ to $80k_B T/r_0$ and a_{AB} changes in the range of $30 \sim 45k_B T/r_0$ in different simulations. The value of a_{sA} evolves from a_{sl} to a_{sb} when the lyophilic segments denature into lyophobic ones, and a_{sB} turns from a_{sb} to a_{sl} during the inversion. Based on the relation established by Groot and Warren²³ for the density $\rho = 3r_0^{-3}$

$$\chi_{ij} = 0.286(a_{ij} - a_{ii})r_0/k_B T, \quad (1)$$

we can estimate the Flory–Huggins parameter between the solvent and the lyophobic block χ_{sb} , the interaction parameter between the solvent and the lyophilic block χ_{sl} and that between *AB* blocks χ_{AB} . The calculated χ_{sb} , χ_{sl} , and χ_{AB} from Eq. (1) are then 4.29–15.73, 0, and 1.43–5.72, respectively, covered in the experimental scale.¹ In experiments, although the core-shell inversion could be induced either by the change of solvent selectivity or by the block denaturation, it is essentially the changed solvent-block interaction parameters that govern the process.

To connect the beads into polymers, spring force \mathbf{F}_{ij}^S is introduced to *A* and *B* beads, with the form $\mathbf{F}_{ij}^S = k(r_{eq} - r_{ij})\mathbf{e}_{ij}$. Previous studies^{23–25} have tried different sets of k and r_{eq} , from $k = 2 \sim 4k_B T/r_0^2$, $r_{eq} = 0$, to $k \approx 161k_B T/r_0^2$, $r_{eq} \approx 0.6r_0$, even to $k \approx 1000k_B T/r_0^2$, $r_{eq} \approx 0.55r_0$. They seem to bring in no apparent discrepancies from the known static or dynamic properties of polymers, except for altering the average bond length. So we choose $k = 64k_B T/r_0^2$ and $r_{eq} = 0.5r_0$ in our simulations. Finally, the equations of Newtonian motion are integrated by a self-consistent leap-frog scheme proposed by Pagonabarraga *et al.*²⁶ This scheme is reported to display better time reversibility and temperature-conserving efficiency than the widely used velocity-Verlet style algorithms.

B. Number of contacts between different species

Section III B will show that different stages in the inversion can be clearly indicated by the number of contacts between the solvent and the blocks. To calculate the value of

these numbers, we firstly divide the simulation box into small lattices of the size $(0.5r_0)^3$. The density distribution of the α bead can be calculated as

$$\rho_\alpha(i,j,k) = \frac{\sum_{n=k-2}^{n=k+2} \sum_{m=j-2}^{m=j+2} \sum_{l=i-2}^{l=i+2} n_\alpha(l,m,n)}{125 \times (0.5r_0)^3} \quad (\alpha = s, A, B),$$

where $n_\alpha(i,j,k)$ is the number of α bead in the lattice (i,j,k) . With such definition, the same bead can be counted for different lattice (i,j,k) . The overcounted bead number is thus rescaled by the factor 125, since there can be 125 neighboring beads that may contribute to the bead number at (i,j,k) . The number of contacts between the bead type α and β is then defined as the number of those lattices with $|\rho_\alpha - \rho_\beta| < 0.5r_0^{-3}$, which means the α and β beads are counted only when they are neighbors of each other,

We note that the number of contacts between the solvent and the blocks defined here is an estimation of the interfacial area between these species. It equals the real area times a coefficient determined by lattice size. Therefore we sometimes use the term ‘‘interfacial area’’ for simplicity, because the lattice size keeps constant throughout the analysis and its value remain proportional to the real area.

C. Hydrodynamic radius

One connection between the simulations and the future experiments of inversion will probably be the instantaneous hydrodynamic radius of the intermediate micellar aggregates, which, together with the radius of gyration, helps reveal the segment arrangements in the intermediate aggregates. Previous studies^{27,28} have applied Zimm’s method²⁹ to evaluating the hydrodynamic quantities of polymers. By virtue of the Monte Carlo generated polymer conformations, the method solved the Kirkwood–Riseman equation³⁰ without invoking the pre-averaging approximation. Here, we combine it with DPD simulations to calculate the hydrodynamic radii of the inversion intermediates, since Zimm’s method requires only the knowledge of all the intersegment distances in an aggregate that the DPD simulation also provide.

Let \mathbf{r}_i be the location of the i th segment (bead) in the micelle, \mathbf{F}_i be the frictional force exerted by the moving segment on the fluid, \mathbf{u}_i be the segment velocity, and \mathbf{v}_i be the fluid velocity at the position \mathbf{r}_i if the segment is removed. The frictional force is induced by the relative motion between the polymer segment and the fluid

$$\mathbf{F}_i = f(\mathbf{u}_i - \mathbf{v}_i), \quad (2)$$

where the frictional coefficient $f = 6\pi\eta a$, a is the Stokes radius of the polymer bead, and η is the fluid viscosity. Reciprocally, the frictional force \mathbf{F}_j exerted by other segment ($j \neq i$) at \mathbf{r}_j gives the velocity disturbance at \mathbf{r}_i through hydrodynamic interactions

$$\mathbf{v}_i = \sum_{j \neq i} \mathbf{T}_{ij} \mathbf{F}_j + \mathbf{v}_{0i}, \quad (3)$$

in which \mathbf{v}_{0i} represents the velocity of external flow at \mathbf{r}_i if the whole micelle is absent. The tensor \mathbf{T}_{ij} , which describes the hydrodynamic effects, is a function of the fluid viscosity

η and of the distance between i and j . We use the simplest form, the Oseen Tensor,

$$\mathbf{T}_{ij} = \frac{1}{8\pi\eta r_{ij}} \left(\mathbf{I} + \frac{\mathbf{r}_{ij} \mathbf{r}_{ij}}{r_{ij}^2} \right),$$

where \mathbf{I} is the unit tensor, although more complex expressions that account the finite size of the segments are available.³¹

Combining Eqs. (2) and (3) together leads to

$$(1/6\pi\eta a) \mathbf{F}_i + \sum_{j \neq i} \mathbf{T}_{ij} \mathbf{F}_j - \mathbf{u}_i = -\mathbf{v}_{0i}. \quad (4)$$

We further apply rigid-body approximation to the intermediate aggregate

$$u_{ix} = u_x - y_i \Omega_z \quad u_{iy} = u_y - x_i \Omega_z \quad u_{iz} = u_z, \quad (5)$$

where $\mathbf{u} = (u_x, u_y, u_z)$ denotes the velocity of the center of mass of the micelle aggregate, and Ω_z is the angular velocity around z -axis. Equations (4) and (5) with $3\mathcal{N}+4$ unknowns (namely, u_x, u_y, u_z, Ω_z , and three components of all \mathbf{F}_i for $i = 1, \dots, \mathcal{N}$) can be solved under the following additional sedimentation conditions:

$$\sum_i \mathbf{F}_i = (0, 0, F_z) = (0, 0, \mathcal{N}k_B T / r_0), \quad (6)$$

$$\mathbf{v}_{0i} = (0, 0, 0), \quad (7)$$

and

$$\Omega_z = 0, \quad (8)$$

where \mathcal{N} denotes the total number of segments in a micellar aggregate. Equation (6) explains an external force along $+z$ direction being applied on the micellar aggregate. The hydrodynamic radius R_h can then be evaluated by

$$R_h = F_z / 6\pi\eta u_z. \quad (9)$$

Previous studies^{23,32} have established the formula for DPD fluid viscosity from the dissipation strength γ and other simulation parameters. In the case that $\gamma = 4.5[(k_B T)m_0/r_0^2]^{1/2}$, $\rho = 3$, and the weight function is of the form given in Sec. II A, the fluid viscosity is $\eta = 0.957(m_0 k_B T)^{1/2} r_0^{-2}$. The choice of the Stokes radius a is more flexible, and the range $a = 0.25 - 0.5r_{eq}$ has been tried and permitted.²⁸ Because Oseen tensor gives a better description of the hydrodynamic interactions when the segment size approaches zero, we set $a = 0.25r_{eq}$ in the simulations.

It should also be noted that solving the large dense non-symmetrical linear equations (4)–(8) is a task consuming considerable time and computational space. We have to run the programs parallel on the IA32 Beowulf clusters.

III. RESULTS AND DISCUSSIONS

A. Inversion dynamics

For clarity and simplicity, the inversion is induced after the micelles are fully equilibrated. Other dynamic processes, such as core relaxation and polymer redistribution between the cores, are decoupled from the inversion process, therefore only the inversion dynamics itself is focused on. How-

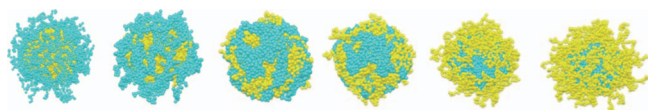


FIG. 1. Morphology evolution during an inversion with zero denaturation time for both types of polymer blocks. The micelle is comprised of 125 block copolymers ($N_A=N_B=N=20$, $\chi_{sb}=7.15$, and $\chi_{AB}=1.43$). As soon as the inversion is induced, the blue A beads in the shell become lyophobic and the yellow B beads in the core turn to be lyophilic. The snapshots, from left to right, correspond to $t=0\tau, 5\tau, 15\tau, 25\tau, 75\tau, 300\tau$.

ever, simulation of micellization from an initial state of randomly scattered copolymers takes place for a time longer than the computers can afford. The computation time is mainly paid for overcoming the potential barriers in unimer entry/expulsion and micelle fusion/fission when small clusters form but the thermodynamically optimal aggregation degree has not been reached.^{18,33} Thus, we initiate the micelle equilibration from a spherical micelle, and let the artificial aggregate relax completely to eliminate any initial effect. In this way, we save amounts of time which would have been spent on adjusting the aggregation degree, i.e., the number of polymers in a micelle.

As a first step, we focus on the simplified inversion by neglecting the time consumed to turn the A -block shell into lyophobic and the B -block core into lyophilic. In other words, both types of blocks complete denaturation instantaneously after the external conditions undergo fast alteration. This can be realized by abruptly raising or lowering the temperature to cause a thermally induced inversion, or by suddenly changing pH value or solvent selectivity when diffusion of small molecules is not a limiting process. In this way the inversion dynamics and the denaturation dynamics are decoupled.

In all the simulations, for each set of parameters, at least four independent runs were performed. The number of solvent molecules is fixed to be 1.92×10^5 and each solvent molecule occupies a volume of $1/\rho$ (with $\rho \approx 3/r_0^3$). The volume of the system is the sum of the volumes of all solvents and the micelle. Since the volume occupied by the solvent molecules is much larger than that of the micelle, the system volume is approximately $1.92 \times 10^5 \times r_0^3/3 = 64 \times 10^3 r_0^3 = (40r_0)^3$, corresponding to a cubic with each edge size equal to 40 nm if one chooses $r_0=1$ nm.

Figure 1 presents the snapshot of a typical simplified inversion process, in which the time needed to convert the lyophobic blocks into lyophilic ones or vice versa is negligible. The polymers in this case consist of A and B blocks with equal length ($N_A=N_B=20$). Apparently, the inversion is in essence the motions of the two types of polymer blocks. Base on the morphology evolution, the process can be roughly divided into two stages, each characterized by the behavior of one type of blocks. In the first stage ($t < 25\tau$ in this case), the agglomeration of A blocks (now they are lyophobic) dominates till the formation of a porous lyophobic layer with finite thickness outside the B -block core (now they are lyophilic). In contrast to the appreciable motions of the A blocks, the B blocks in this period just swell a little. The second stage ($t > 25\tau$) is characterized by the penetration of

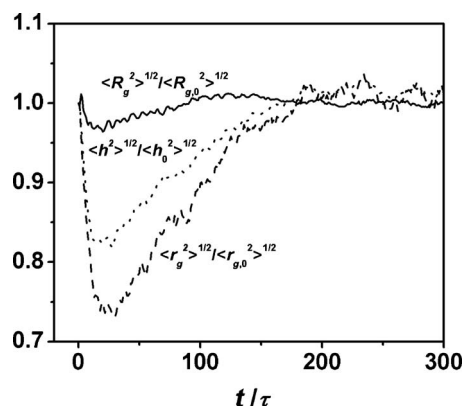


FIG. 2. The time evolutions of the gyration radius of the micelle $\langle R_g^2 \rangle^{1/2}$, the end-to-end distance $\langle h^2 \rangle^{1/2}$ and the gyration radius $\langle r_g^2 \rangle^{1/2}$ of the constituent block copolymers. $\langle R_{g,0}^2 \rangle^{1/2}$, $\langle h_0^2 \rangle^{1/2}$, and $\langle r_{g,0}^2 \rangle^{1/2}$ are the corresponding equilibrated values of $\langle R_g^2 \rangle^{1/2}$, $\langle h^2 \rangle^{1/2}$, and $\langle r_g^2 \rangle^{1/2}$, respectively. Minima appear around 25τ for all three properties. The micelle is comprised of 125 block copolymers ($N_A=N_B=N=20$, $\chi_{sb}=7.15$, and $\chi_{AB}=1.43$).

the B blocks through the lyophobic A -block layer, which continues to collapse centripetally to avoid the contact with solvent beads.

The evolutions of the micellar radius of gyration and the constituent copolymer conformations are shown in Fig. 2, which also indicates the distinction between the two stages. Firstly, the fast and large-scale agglomeration of the A blocks together with the slow and slight swelling of the B -block core result in rapid shrinking in micelle size and coiling of its copolymers. This process completes fast because initially the A -block shell is loose, thus the polymer chains are easier to adjust their conformation. After the fast collapse of the A -shell, the number of the B blocks that pass through the dense A -block layer and extend into the solvent gradually increases. Thus the second stage is the rate limiting stage of the whole inversion process. The flowing of B beads through the thick A -layer requires the disentanglement of the chains, and hence slows down the whole process. In Fig. 2, the completion of the second stage is featured by the return to the original values of the three properties after the minima around 25τ .

Similarly, we observe a peak in the $\langle R_g^2 \rangle^{1/2}/\langle R_h \rangle$ curve in Fig. 3 at $t \approx 25\tau$, the dividing point that separates the two

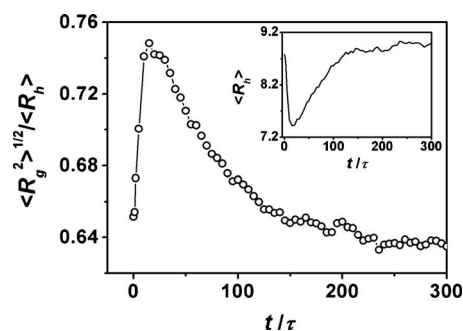


FIG. 3. The time evolution of $\langle R_g^2 \rangle^{1/2}/\langle R_h \rangle$. Maximum appears around $t = 25\tau$. The inset is the instantaneous hydrodynamic radii $\langle R_h \rangle$ for the inversion intermediates, whose shape is similar to the curve of $\langle R_g^2 \rangle^{1/2}$ evolution. The micelle is comprised of 125 block copolymers ($N_A=N_B=N=20$, $\chi_{sb}=7.15$, and $\chi_{AB}=1.43$).

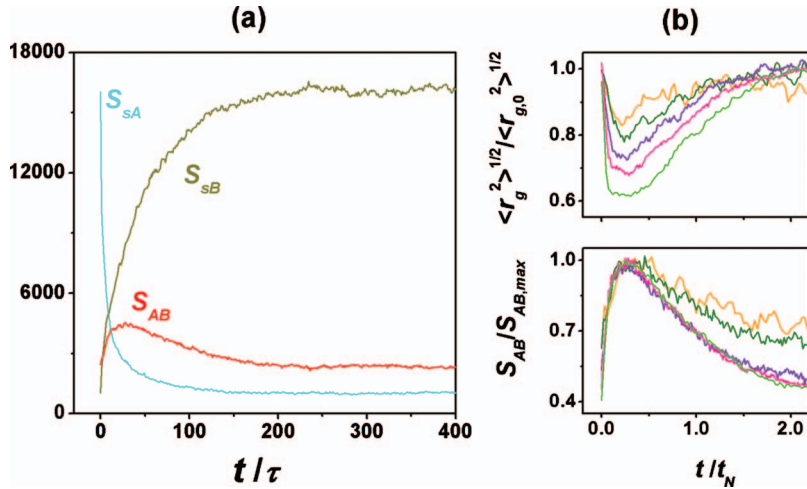


FIG. 4. (a) The evolutions of number of contacts (interfacial area) between the solvent and the inward-moving A blocks S_{SA} (azure line), the contacts between the solvent and the outward-moving B blocks S_{SB} (yellow line) and that between the two types of blocks S_{AB} (red line) for the micelles of 125 block copolymers ($N_A=N_B=N=20$, $\chi_{sb}=7.15$, and $\chi_{AB}=1.43$). (b) The evolutions of the renormalized S_{AB} and the gyration radii of the constituent copolymers $\langle r_g^2 \rangle^{1/2}$ for micelles whose constituent copolymers are of the block length $N=5$ (orange line), 10 (olive line), 20 (violet line), 40 (pink line), and 80 (green line), respectively.

stages in this typical inversion process. The hydrodynamic radius, $\langle R_h \rangle$, is defined as the size of the equivalent hard sphere that moves with the same velocity as the micelle in the solvent. For a rigid uniform sphere, $\langle R_g^2 \rangle^{1/2} / \langle R_h \rangle$ is a constant, 0.775, according to the formula

$$\langle R_g^2 \rangle = \frac{\int_0^{R_h} 4\pi r^2 \cdot r^2 \cdot \rho dr}{\int_0^{R_h} 4\pi r^2 \cdot \rho dr} = (0.775R_h)^2.$$

In nonuniform aggregates, either decrease in the core density or increase in the shell density raises $\langle R_g^2 \rangle^{1/2} / \langle R_h \rangle$; any opposite alterations, including densifying the core and diluting the shell, lead to a decreased $\langle R_g^2 \rangle^{1/2} / \langle R_h \rangle$. When $t < 25\tau$, it is obvious that agglomeration of A blocks creates a denser shell and the core density is reduced somewhat by swelling. So $\langle R_g^2 \rangle^{1/2} / \langle R_h \rangle$ rises all the way in the first stage. As $t > 25\tau$, the lyophobic layer moves inwards and gradually substitutes for the swelled lyophilic B-block core. Consequently, $\langle R_g^2 \rangle^{1/2} / \langle R_h \rangle$ falls until reaching the equilibrium value before inversion. The peak around 25τ indicates the formation of the inversion intermediate with a denser shell and a diluter core.

A typical inversion lasts up to 300τ in the simulations. If we equate the simulated diffusion coefficient of polymer $2-8r_0^2/\tau$ with the experimental scale 10^{-12} m²/s in dilute regime and 10^{-14} m²/s in concentrated regime,³⁴ and assume $r_0 \approx 1$ nm,^{21,23,25} then the simulation time scale varies in the range of $\tau \approx 10^{-6}-10^{-4}$ s. We estimate the mapped experimental inversion time t_{expt} from the relation $R_{g,\text{sim}}^2/300\tau \approx R_{g,\text{expt}}^2/t_{\text{expt}}$ with $R_{g,\text{sim}} \approx 5.7 r_0$ and $R_{g,\text{expt}} \approx 20$ nm. The result is $t_{\text{expt}} \approx 10^{-2}-1$ s, a bit smaller than that observed in the experiments.^{15,16} Many factors can be attributed to the acceleration in our simulation, including (1) decoupling with intermicelle interactions, fusion/fission and unimer entry/expulsion and (2) that the soft interbead potentials, which permit bead overlaps, diminish the entanglements in a many-chain system. Since the molecular weights¹⁻¹⁷ of the polymeric amphiphiles for micelles are always in the range of 10^3-10^5 where few entanglements are produced, we consider the simulation results approach closer to the time scale of a pure inversion event.

B. Characteristic time of inversions

This section is concentrated on the determination of the inversion time scale. Firstly, how can the completing point of the inversion be defined, since the progress goes slower as it approaches the end? Compared with the rugged curves of $\langle R_g^2 \rangle^{1/2}$ and $\langle h^2 \rangle^{1/2}$ in Fig. 2, the number of contacts (interfacial areas) between different components in the system evolves more smoothly. So we use this number to determine the time scale of inversion. Figure 4(a) shows the evolutions of interfacial areas between different components in the system shown in Fig. 1. The interfacial area between A and B blocks S_{AB} increases and then reaches the maximum around 25τ . Similar to Figs. 2 and 3, both the solvent-A interfacial area S_{SA} and the solvent-B interfacial area S_{SB} change fast in the first stage ($t < 25\tau$), and slow down afterwards. The closer as the structure approaches the equilibrium state, the slower the B blocks flow through the thick lyophobic A-block layer. The asymptotic behavior sweeps off the possibility of setting the end point of the inversion. So the time needed for S_{SB} to reach 90% of its equilibrated value is taken to characterize the inversion time scale, denoted as t_N . We plot the values of $S_{AB}/S_{AB,max}$ and $\langle r_g^2 \rangle / \langle r_{g,0}^2 \rangle$ of the micellar aggregates with different constituent-polymer lengths against the normalized time t/t_N , and observe that all the maxima or minima appear at $t/t_N \approx 0.23$ for all N [Fig. 4(b)]. The overlapped peaks indicate determining t_N partially based on S_{SB} introduces no partiality in measuring the overall inversion time. It is equivalent to the characteristic time defined as the time, t_M , taken for S_{AB} to reach the maximum or for $\langle r_g^2 \rangle^{1/2}$ to go down to the nadir. For any N , the characteristic time times, t_N and t_M , which are defined differently, can be converted to each other by multiplying a same proportional coefficient.

Figure 5 presents the dependence of the characteristic time of inversion on the block length of the constituent copolymers. It shows there is a scaling relation $t_N \sim N^\alpha$, with the scaling exponent $\alpha \approx 1.67-1.89$ (if the scaling is performed in terms of $N-1$, slightly lower exponent $\alpha \approx 1.52-1.73$ is obtained). It is interesting to discuss why the scaling exponent takes such value. If one assumes the polymers undergo Brownian motion, the inversion time scale is

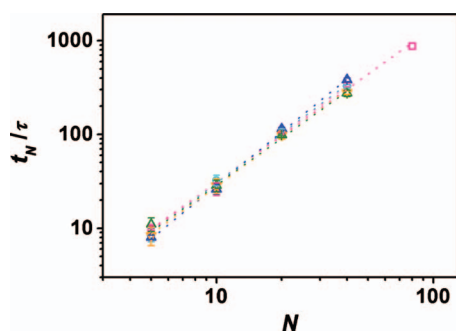


FIG. 5. Dependence of the characteristic inversion time on the block length of the constituent copolymers. The points are the simulated data and the dotted lines are fitted. (Pink: $\chi_{AB}=1.43$, $\chi_{sb}=7.15$, fitted slope is 1.72 ± 0.08 if only the first four points are taken into account and 1.65 ± 0.06 including the last point for $N=80$; azure: $\chi_{AB}=1.43$, $\chi_{sb}=4.29$, fitted slope is 1.75 ± 0.05 ; blue: $\chi_{AB}=1.43$, $\chi_{sb}=12.87$, fitted slope is 1.89 ± 0.05 ; orange: $\chi_{AB}=3.58$, $\chi_{sb}=7.15$, fitted slope is 1.70 ± 0.04 ; olive: $\chi_{AB}=5.72$, $\chi_{sb}=7.15$, fitted slope is 1.67 ± 0.06).

determined by the relation $t_N \sim R_g^2/D$, where D is the diffusion coefficient of polymer. The polymer concentration near or within a micelle is in the regime where the hydrodynamic interactions have been screened, so it is reasonable to assume D obeys Rouse dynamics,³⁵ thus $D \sim N^{-1}$. Using the simulation data $R_g \sim N^{0.67}$ (for the system $\chi_{AB}=1.43$, $\chi_{sb}=7.15$) leads to the scaling exponent $\alpha \approx 2.3$, which is apparently larger than the simulated results. Therefore, it can be affirmed that the inversion events would be completed more slowly if there were only random movements of the polymer segments with no driving force incorporated.

We thus apply another model to simplify the understanding of the complex inversion process. The model assumes that in the inversion the polymer segments move from a region of high chemical potential to a region of low chemical potential. It is also a simplified translocation model with the entropic changes neglected and the free energy barriers absent.^{36,37} Initially, N segments are confined in the thermodynamically unfavorable side. There are no chain connections between the segments and they move totally independently. Each segment tends to enter the other lower-chemical-potential side with the same mobility. The time scale of the chemical-potential driven flow is then³⁶

$$t_N \propto \frac{N}{|\Delta\mu|} \left\{ 1 - \frac{k_B T}{N|\Delta\mu|} \left[1 - \exp\left(-\frac{N|\Delta\mu|}{k_B T}\right) \right] \right\}, \quad (10)$$

where $\Delta\mu < 0$ denotes the chemical potential difference between the two regions. For extremely short chains, $t_N \sim N^2$; while for micelles consist of sufficiently long copolymers, $t_N \sim N$. In the N range of 10–100, curves of Eq. (10) can be approximated by a scaling relation $t_N \sim N^{1.6-1.9}$ for all $\Delta\mu$, close to the simulation results. It is a revelation that the segment flow driven by the incompatibility between the denatured blocks and their surroundings is the essence of the inversion process, despite of the various appearances of intermediate aggregate morphologies and polymer conformations.

Some literatures^{38,39} have discussed the inconsistency in the application of Eq. (10) to the translocation of a polymer. However, it should be pointed out that Eq. (10), as a model

of forced Brownian motion, has no innate problems, and the equilibrium assumption for each state under which Eq. (10) is derived holds. Inconsistency emerges only when Eq. (10) is used to predict the behaviors of the system in which the detailed balance is not applied to, such as long polymer chains. Since the equilibration time of Rouse chain scales as $N^{2\nu+1}$ (ν is Flory exponent), the time needed for equilibration will eventually exceed the time scale predicted by Eq. (10) as the chain becomes longer. So the equilibrium assumption fails and $t_N \sim N$ does not hold for large N . For the long chains, the time scale of their forced motion with no barriers is supposed to be the lower boundary, and should not be overtaken by other forced motions experiencing barriers (such as the entropic barrier in translocation through a hole, or the interdiffusion of each type of blocks through the other in micelle inversion). The boundary can be calculated by $t_{LB} \sim R_g/u \sim R_g N/\Delta\mu \sim N^\beta/\Delta\mu$, where u is the velocity of the chain's center of mass. $\beta \approx 1.67$ if the simulation data for $\chi_{AB}=1.43$ and $\chi_{sb}=7.15$ are used, and β is always larger than 1.5 if other sets of the interaction parameters are employed.

C. Comparison with experiments

To simplify the analysis of the inversion dynamics, we have assumed that the two blocks instantaneously achieve complete denaturation following the change of external conditions, thus decoupling the inversion and denaturation dynamics. This is valid in the experiments where the temperature jumps abruptly to cause thermally induced inversion or molecule diffusion is not a limiting factor in the inversion triggered by pH or solvent selectivity. When the molecular diffusion is a limiting process, however, this decoupling may not always be applicable. Therefore, we have also simulated the inversion dynamics with various denaturation times of the blocks A and B . The conclusion is that enlarging the denaturation time of the initially core-forming block B over that of the shell-forming block A produces smooth, tight-wrapped intermediates; whereas rugged, or even scattered intermediates are yielded if the block A denaturation time exceeds the block B . A typical result is shown in Fig. 6, where the denaturation time of the initially shell-forming block A is systematically elongated from 25τ , 50τ , to 110τ , while the denaturation time of block B is fixed to zero. As is shown in Fig. 6, only when the block A denaturation time (greater than 50τ) is significantly longer than block B , dispersed intermediates appear, because the small clusters will diffuse sufficiently far away to escape the association region of B blocks before the reunification of the lyophobic A blocks. Since the solvent molecules or the ions pass sequentially through the outer A -block shell and then the inner B -block core, there are hardly the cases that the core denatures faster by far than the shell. We therefore expect no molecularly dispersed intermediates exist in most of the inversion experiments on the spherical micelles comprised of symmetric diblock copolymers. A similar conclusion has already been drawn by Chen *et al.*,² when they compared the morphological changes of PS-P4VP micelles after the continuous and the discontinuous switching of the solvent selectivity.

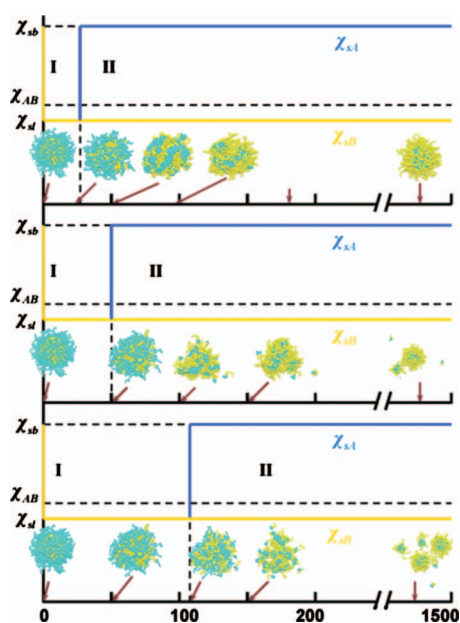


FIG. 6. Morphology evolutions during inversions with the denaturation times of block A changing from 25τ , 50τ , to 110τ , while the denaturation time of block B is fixed to zero. The micelle is comprised of 125 block copolymers ($N_A=N_B=N=20$, $\chi_{sb}=7.15$, and $\chi_{AB}=1.43$). The solid blue and yellow lines represent the evolution profiles of the interaction parameter between the solvent and block A and that between the solvent and block B, respectively. The dashed lines are guide to the eyes. The brown arrows indicate the time at which the snapshots are taken.

Liu *et al.* have investigated the inversion kinetics of two micellar systems composed of pH-responsive¹⁵ and salt-responsive¹⁶ asymmetric diblock copolymers, respectively. Initial decrease in the time dependent curves of the light scattering intensity has been observed during the pH-induced inversion from the small-core micelles into the large-core ones and the salt-induced inversion from the large-core micelles into the small-core ones. They consider the decrease should be due to the immediate dissociation of the micelles into unimers. However, the simulations indicate molecularly scattered state hardly appears in an inversion. Thus there may be an alternative explanation to Liu's experiments. The intensity decrease can be an indication of the formation of the semi-scattered clusters with loosely associated lyophilic blocks (Fig. 6), rather than the complete scattered states of unimers. Furthermore, we find that micelle disintegration only takes place when the denaturation time of block A significantly exceeds that of block B, as shown in Fig. 6. Thus, the intensity reduction in the experimental inversions probably tells that the blocks in shell move inwards slower than the core blocks move outwards.

IV. CONCLUSIONS

Our simulations on the inversion dynamics of micelles composed of symmetric block copolymers aim to a deeper understanding of the dynamic event. We observe from the time-dependent morphology that the micellar aggregates keep strong or weak association throughout the whole process, and do not experience any molecularly scattered intermediate states for most inversions. The only exception appears when experimental conditions are deliberately

controlled to induce faster core dispersion. Two correlated motions have also been distinguished by monitoring the morphology and other quantitative parameters. They are the faster agglomeration of the inward-moving blocks, which dominates the early stage of the inversion, and the slow swelling and penetration through a lyophobic layer of the outward-moving blocks, which dominates the later stage of the inversion. Simulations on the inversion with various denaturation times have also been conducted. Intermediates with denser shell and diluter core are formed in all the inversion processes, revealed by the raised peak in the evolution curve of $\langle R_g^2 \rangle^{1/2} / \langle R_h \rangle$.

A scaling relation between the inversion time and the polymer chain length is observed with a scaling exponent ranging at 1.67–1.89. A simplified model of a chemical-potential-driven Brownian motion of polymer segments is introduced to analyze the value of the exponent. However, more detailed models can be constructed to account for the effect of other factors, e.g., local densification of one type of blocks, whose involvement certainly complicates the situation. Moreover, the conformational change of the constituent copolymers is also fascinating and deserves further analytical study.

We note that introducing the harmonic potential between connected beads cannot prevent bond crossing. However, for relatively short chains, the dynamics of polymers in melt state is typically described by the Rouse dynamics, allowing bond crossing is not a problem. For longer chains, introducing reptational dynamics in DPD is possible, as shown in a recent paper by Nikunen *et al.*⁴⁰ Nonetheless, even if uncrossability of chains is enforced, we believe the kinetics will remain qualitatively the same.

In the present simulation another oversimplification may be the isolation of the individual micelles from their neighbors. Consequently, intermicellar interactions are excluded from our simulation. Thus our simulation is valid in a dilute micelle solution, in which the fusion among micelles is not significant. We may estimate the time scale of the intermicellar collision at $t=L^2/6D$ and $L=(N_A c_{mic})^{-1/3}$, where L is the average intermicellar distance, N_A is the Avogadro constant, and c_{mic} is the mole concentration of micelles. The diffusion coefficient of micelles D can be derived from the Stokes–Einstein equation. If we input the parameters of the inversion systems investigated by Liu *et al.*^{15,16} into the formulae, the estimated mean time of collision varies in 10^{-2} –1 ms, much shorter than the simulated times (10^{-2} –1 s) and the experimental scales (1–10 s). So the intermicellar interaction, such as collision and fusion, are always present. Although the fusion does not necessarily accompany the inversion and could be neglected in a first investigation, the effects of the intermicellar interaction on the inversion dynamics certainly deserve a future simulation.

ACKNOWLEDGMENTS

We thank Professor Daoyong Chen for inspiring discussions. We are grateful to the financial support from the National Basic Research Program of China (Grant No. 2005CB623807) and National Natural Science Foundation of

China (Grant Nos. 20625413, 20874021, and 20990231). We are also grateful to the Supercomputing Center of Fudan University where the simulations were run on IA32 Beowulf clusters.

- ¹I. W. Hamley, *The Physics of Block Copolymers* (Oxford University Press, Oxford, 1998).
- ²G. L. Hou, L. Zhu, D. Y. Chen, and M. Jiang, *Macromolecules* **40**, 2134 (2007).
- ³J. M. V. Weaver, S. P. Armes, and V. Bütün, *Chem. Commun. (Cambridge)* **2002**, 2122.
- ⁴Y. Maeda, H. Mochiduki, and I. Ikeda, *Macromol. Rapid Commun.* **25**, 1330 (2004).
- ⁵S. Y. Liu, N. C. Billingham, and S. P. Armes, *Angew. Chem., Int. Ed.* **40**, 2328 (2001).
- ⁶J. Virtanen, M. Arotcarena, B. Heise, S. Ishaya, A. Laschewsky, and H. Tenhu, *Langmuir* **18**, 5360 (2002).
- ⁷S. Y. Liu and S. P. Armes, *Angew. Chem., Int. Ed.* **41**, 1413 (2002).
- ⁸V. Bütün, S. P. Armes, N. C. Billingham, Z. Tuzar, A. Rankin, J. Eastoe, and R. K. Heenan, *Macromolecules* **34**, 1503 (2001).
- ⁹S. Dai, P. Ravi, K. C. Tam, B. W. Mao, and L. H. Gan, *Langmuir* **19**, 5175 (2003).
- ¹⁰V. Bütün, N. C. Billingham, and S. P. Armes, *J. Am. Chem. Soc.* **120**, 11818 (1998).
- ¹¹Y. L. Cai and S. P. Armes, *Macromolecules* **37**, 7116 (2004).
- ¹²V. Bütün, R. B. Top, and S. Ufuklar, *Macromolecules* **39**, 1216 (2006).
- ¹³J. Rodríguez-Hernández and S. Lexommandoux, *J. Am. Chem. Soc.* **127**, 2026 (2005).
- ¹⁴C. Allen, D. Maysinger, and A. Eisenberg, *Colloids Surf., B* **16**, 3 (1999).
- ¹⁵D. Wang, J. Yin, Z. Y. Zhu, Z. S. Ge, H. W. Liu, S. P. Armes, and S. Y. Liu, *Macromolecules* **39**, 7378 (2006).
- ¹⁶D. Wang, T. Wu, X. J. Wan, X. F. Wang, and S. Y. Liu, *Langmuir* **23**, 11866 (2007).
- ¹⁷F. T. Liu and A. Eisenberg, *J. Am. Chem. Soc.* **125**, 15059 (2003).
- ¹⁸E. A. G. Aniansson and S. N. Wall, *J. Phys. Chem.* **78**, 1024 (1974); E. A. G. Aniansson and S. N. Wall, *ibid.* **79**, 857 (1975); E. A. G. Aniansson, S. N. Wall, M. Almgren, H. Hoffmann, I. Kielmann, W. Ulbricht, R. Zana, J. Lang, and C. Tondre, *ibid.* **80**, 905 (1976).
- ¹⁹P. J. Hoogerbrugge and J. M. V. A. Doelman, *Europhys. Lett.* **19**, 155 (1992).
- ²⁰P. De Palma, P. Valentini, and M. Napolitano, *Phys. Fluids* **18**, 027103 (2006); M. Whittle and E. Dickinson, *J. Colloid Interface Sci.* **242**, 106 (2001).
- ²¹R. D. Groot and K. L. Rabone, *Biophys. J.* **81**, 725 (2001); M. Laradji and P. B. S. Kumar, *Phys. Rev. Lett.* **93**, 198105 (2004).
- ²²Y. Kong, C. W. Manke, and W. G. Madden, *J. Chem. Phys.* **107**, 592 (1997).
- ²³R. D. Groot and P. B. Warren, *J. Chem. Phys.* **107**, 4423 (1997).
- ²⁴W. H. Jiang, J. H. Huang, Y. M. Wang, and M. Laradji, *J. Chem. Phys.* **126**, 044901 (2007).
- ²⁵V. Ortiz, S. O. Nielsen, D. E. Discher, M. L. Klein, R. Lipowsky, and J. Shillcock, *J. Phys. Chem. B* **109**, 17708 (2005).
- ²⁶I. Pagonabarraga, M. H. J. Hagen, and D. Frenkel, *Europhys. Lett.* **42**, 377 (1998); I. Vattulainen, M. Karttunen, G. Besold, and J. M. Polson, *J. Chem. Phys.* **116**, 3967 (2002).
- ²⁷M. K. Wilkinson, D. S. Gaunt, J. E. Lipson, and S. G. Wittington, *Macromolecules* **21**, 1818 (1988).
- ²⁸K. Shida, K. Ohno, M. Kimura, Y. Kawazoe, and Y. Nakamura, *Macromolecules* **31**, 2343 (1998).
- ²⁹B. H. Zimm, *Macromolecules* **13**, 592 (1980).
- ³⁰J. G. Kirkwood and J. Riseman, *J. Chem. Phys.* **16**, 565 (1948).
- ³¹J. Rotne and S. Prager, *J. Chem. Phys.* **50**, 4831 (1969); H. Yamakawa, *ibid.* **53**, 436 (1970).
- ³²C. A. Marsh, G. Bachx, and M. H. Ernst, *Europhys. Lett.* **38**, 411 (1997); A. Satoh and T. Majima, *J. Colloid Interface Sci.* **283**, 251 (2005).
- ³³E. E. Dormidontova, *Macromolecules* **32**, 7630 (1999).
- ³⁴U. K. Ghosh, S. Kumar, and S. N. Upadhyay, *J. Chem. Eng. Data* **36**, 413 (1991); J. Kanatharana, J. Sukpisan, A. Sirivat, and S. Q. Wang, *Polym. Eng. Sci.* **36**, 2986 (1996); N. Nemoto, T. Kojima, T. Inoue, M. Kishine, T. Hirayama, and M. Kurata, *Macromolecules* **22**, 3793 (1989).
- ³⁵M. Doi and S. F. Edwards, *The Theory of Polymer Dynamics* (Clarendon, Oxford, 1986).
- ³⁶M. Muthukumar, *J. Chem. Phys.* **111**, 10371 (1999).
- ³⁷M. Muthukumar, *Phys. Rev. Lett.* **86**, 3188 (2001).
- ³⁸A. Cacciuto and E. Luijten, *Phys. Rev. Lett.* **96**, 238104 (2006).
- ³⁹J. Chuang, Y. Kantor, and M. Kardar, *Phys. Rev. E* **65**, 011802 (2001); Y. Kantor and M. Kardar, *ibid.* **69**, 021806 (2004).
- ⁴⁰P. Nikunen, I. Vattulainen, and M. Karttunen, *Phys. Rev. E* **75**, 036713 (2007).